Journal of Chromatography A, 1218 (2011) 2252–2263

Contents lists available at ScienceDirect

Journal of Chromatography A

journal homepage: www.elsevier.com/locate/chroma

Modelling the thermal behaviour of the Low-Thermal Mass Liquid Chromatography system

Matthias Verstraeten[a], Matthias Pursch[b], Patric Eckerle[b], Jim Luong[c], Gert Desmet[a,*]

[a] Vrije Universiteit Brussel, Department of Chemical Engineering, Pleinlaan 2, 1050 Elsene, Belgium
[b] Dow Deutschland GmbH, Analytical Technologies, 77836 Rheinmunster, Germany
[c] Dow Canada, Analytical Technologies, Fort Saskatchewan, AB, Canada

ARTICLE INFO

Article history:
Received 16 December 2010
Received in revised form 3 February 2011
Accepted 9 February 2011
Available online 16 February 2011

Keywords:
Temperature
Temperature programming
Low-Thermal Mass LC
Heat transfer
Band broadening
Mobile phase pre-heating

ABSTRACT

We report upon the experimental investigation of the heat transfer in low thermal mass LC (LTMLC) systems, used under temperature gradient conditions. The influence of the temperature ramp, the capillary dimensions, the material selection and the chromatographic conditions on the radial temperature gradients formed when applying a temperature ramp were investigated by a numerical model and verified with experimental temperature measurements. It was found that the radial temperature gradients scale linearly with the heating rate, quadratically with the radius of the capillary and inversely to the thermal diffusivity. Because of the thermal radial gradients in the liquid zone inside the capillary lead to radial viscosity and velocity gradients, they form an additional source of dispersion for the solutes. For a temperature ramp of 1 K/s and a strong temperature dependence of the retention of small molecules, the model predicts that narrow-bore columns (i.d. 2.1 mm) can be used. For a temperature ramp of 10 K/s, the maximal inner diameter is of the order of 1 mm before a substantial increase in dispersion occurs.

1. Introduction

All current trends in LC aim at obtaining faster separations and higher resolutions. The evolution in LC equipment and techniques includes the use of smaller particles [1,2] and the consequent use of higher pressures [3], the reduction of extra-column band broadening [4] and the use of high temperature-LC (HTLC) [5–8]. The latter has been introduced because both the mobile phase viscosity and the retention decrease with increasing temperature, allowing faster separations and the enhancement of diffusion at higher temperatures leads to an increase in efficiency in the high linear velocity range.

The use of higher temperatures however also has some disadvantages. Stationary phases such as the traditional C_{18} coated Si-particles are not thermally stable at high temperatures and a significant decrease of performance over time can be noted. The development of new stationary phases is in full progress and stable packing materials for temperatures up to 200 °C have been reported [9,10]. Also the thermal environment of the column is of major importance and has a large influence on the column efficiency. The mobile phase has to be pre-heated in order to avoid thermal mismatch between the entering liquid and the column temperature. This would induce thermal gradients and leads to radial trans-column viscosity and velocity gradients, enhancing the dispersion of solutes [11,12]. Wolcott et al. reported that a thermal mismatch larger than 6 °C will lead to an excessive contribution to band broadening for a 4.6 mm i.d. column [13]. Besides the mobile phase pre-heating issue, the thermal boundary conditions of the column also play an important role. When the column wall is kept isothermal (e.g., in a water bath), radial temperature gradients will be formed when the column is not in thermal equilibrium with its environment, leading to the development of a radial trans-column velocity profile, in turn introducing a drastic drop in column efficiency [11,14,15]. When the column is operated adiabatically (e.g., insulated column wall), mainly axial temperature gradients will be formed and only a minor decrease in column efficiency will be observed [16,17]. The higher temperatures at the end of the column however might result in some loss of retention capacity. In practice, still- or forced-air ovens are used and the thermal state of the column lies between the isothermal and adiabatic case [16].

Another well-known way to improve the separation resolution in chromatography is the use of gradient elutions, such as gradient elution in LC and temperature programming in GC. In reversed-phase LC, the retention and selectivity are modulated with a solvent gradient which starts with a weak solvent after which the retention of the solutes is decreased by gradually adding more organic modifier to obtain a stronger solvent [18]. Equivalently, temperature programming in GC is obtained by increasing the column temperature during the analysis run and the retention will drastically decrease with increasing temperature.

* Corresponding author. Tel.: +32 02 629 32 51; fax: +32 02 629 32 48.
E-mail address: gedesmet@vub.ac.be (G. Desmet).

0021-9673/$ – see front matter © 2011 Elsevier B.V. All rights reserved.
doi:10.1016/j.chroma.2011.02.023

In the early days of LC, temperature programming was scarcely investigated because the retention and selectivity are less temperature sensitive in the liquid phase compared to the gas phase [19]. Additionally, columns of conventional wide- and normal-bore dimensions have a high thermal mass and rapid temperature changes will lead to radial thermal gradients, in turn known to reduce the column efficiency. In the mid 1990s, Chen and Horvath implemented temperature programming in LC, using a 180 μm i.d. fused-silica capillary packed with 6 μm C_{18}-silica particles to investigate the effect of temperature programming in a separation of alkylbenzenes and in a separation of proteins [20]. The two modes of anisocratic elution were compared and it was found that temperature programming is only a weak alternative for gradient elution because 50 °C change in temperature only corresponded to 10% change in acetonitrile (alkylbenzenes, range: 30–80 °C). Guillarme et al. showed similar results, showing that the shift in retention time induced by an increase of temperature of 30–50 °C can already be achieved by a modest 10% increase of organic fraction [6]. However, Chen and Horvath proposed that the use of temperature programming in combination with gradient elution could be used to fine-tune the retention and increase the resolution of closely related macromolecules such as the proteins.

A recent example by Vanhoenacker and Sandra showed that a mixture of ten triazine and ten phenylurea pesticides could only be baseline separated with the use of temperature programming supplementary to gradient elution [10]; other examples of the use of temperature programming can be found in [21–24]. The advantages of the combined use of gradient elution and temperature programming were also pointed out by Djordjevic and co-workers [25] and by the group of Nikitas and Pappa-Louisi who discussed the simultaneous optimization of the elution gradient and the temperature program [26–28]. Applications in diverse domains such as the separation of polymers, pharmaceuticals, environmental analyses, structural isomers, peptides, proteins and nucleotides have been demonstrated by numerous groups [29–34].

In practice, most setups use a GC or LC oven for temperature programming [21], but other instrumentation can be found in literature, such as the Polaratherm™ oven [35] or the HT-HPLC 200 Column Oven™ [36], circulating baths, block-heating ovens or heating tapes [35–39]. The custom built LC-programmable oven from Spark Holland is equipped with Peltier elements for negative temperature programming, but a poor cooling capacity is reported [40]. The main drawback of these different ovens and setups is that they are limited to temperature ramps of 30 °C/min [35,36] because the degree of heating depends on how fast the air/liquid can be heated in a GC oven/heating bath, or on the quality of thermal contact with the column in a heating block oven.

A novel design of a GC heating module was recently introduced where a nickel wire is wounded around the GC capillary column for resistive heating [41,42]. The low thermal mass of the setup and the principle of resistive wire heating were able to deliver temperature ramps up to 1800 °C/min with a high accuracy, as well as cooling rates up to 400 °C/min for a capillary of 100 μm i.d. and 2 m length. Additionally, low power consumption and a very good repeatability (retention time precision and area count) were reported. This technique was extended and implemented for LC where the fused silica capillary column is inserted into an aluminium tube that is resistively heated and controlled by a Low Thermal Mass (LTM) assembly [23]. To facilitate the heat transport through the capillary column, no polymer or metal capillaries were considered due to their low thermal conductivity and/or high thermal mass. For a packed silica capillary column with an inner diameter of 500 μm, temperature ramps up to 1800 °C/min and cooling rates of 100–200 °C/min were obtained. This setup also allows different columns to be changed very rapidly (in contrast to the LTMGC module), as long as the inner diameter of the aluminium heating sleeve exceeds the outer diameter of the silica column. The potential of the Low-Thermal Mass-LC (LTMLC) technology for fast and ultra-fast separations has been shown in [23] for a number of analyte classes.

The aim of the present study is to study the heat transfer in the current LTMLC setup and to investigate whether it can be improved. To fully understand the effects of different parameters such as the geometry, temperature ramp, flow rate, mobile phase preheating and material selection, the heat transfer equations were numerically solved and the results were validated by experimental measurements of the temperature of the liquid at the capillary's outlet. The present contribution also discusses the scaling-up of the system and investigates the influence of the capillary's inner diameter, mobile phase solvent and the temperature ramp on the radial temperature profiles in the column and their contribution to the extra band broadening.

2. Theoretical framework

2.1. Analytical temperature distribution in an infinitely long cylinder with heated outer wall

The most simplified model one can conceive of to represent the LTMLC-system consists of an infinitely long cylinder with uniform properties and a heated outer wall (schematically represented in Fig. 1a). In this crude approximation of the true annular layer structure of the LTMLC-system (see Fig. 1b for a more detailed cross-section), the heat conduction properties of the different material layers are lumped into one single "black box" material. In addition, the cylinder model also neglects the axial flow through the system. Nevertheless, as will become clear in Section 4, the infinitely long cylinder model provides a good first principles insight into the real problem. The main advantage of the model is that it is amenable to an analytical solution for the radial temperature distribution one can expect as a response to a process wherein the outer cylinder wall is heated at a constant temperature ramp β (K/s). This solution is given by [43]:

$$T(r) = T_0 + \beta\left(t - \frac{R^2 - r^2}{4\alpha}\right) + \frac{2\beta}{R\alpha}\sum_{n=1}^{\infty} e^{-\alpha\lambda_n^2 t}\frac{J_0(r\lambda_n)}{\lambda_n^3 J_1(R\lambda_n)} \quad (1)$$

wherein $\lambda_n = \zeta_n/R$ and ζ_n is the nth root of $J_0(\zeta_n) = 0$, which can be calculated with standard numerical methods or found in [44,45]. α (m^2/s) is the thermal diffusivity of the material, which is the ratio of the thermal conductivity coefficient λ (W/m K) to the thermal mass $C_{p,v}$ (J/m^3 K). T_0 is the uniform initial temperature of the cylinder with outer radius R. Eq. (1) is only valid for a cylinder in which the axial flow can be neglected.

2.2. Band broadening due to thermal effects

The heating of the capillary's wall imposes a radial temperature gradient in the liquid which leads to a radial viscosity gradient, which in turn leads to a radial velocity gradient and thus to an additional source of band broadening [11,14,15,46,47]. In the present study, the viscosity profile was calculated from the known temperature profile using the empirical Vogel equation [48–50]:

$$\eta(r) = \eta(T(r)) = A10^{(B/(T(r)-C))} \quad (2)$$

wherein η is the viscosity in Pa s. For water, the coefficients A, B and C equal 2.414×10^{-5} Pa s, 247.8 K and 140 K respectively [51]. For methanol and acetonitrile, the coefficients are obtained from the fitted data in [52]. For methanol, the coefficients equal 7.463×10^{-4} Pa s, 547.3 K and 4.4 K respectively and for acetonitrile, the coefficients equal 1.120×10^{-3} Pa s, 528.8 K and −59.5 K respectively. Assuming a linear inverse relationship between viscosity

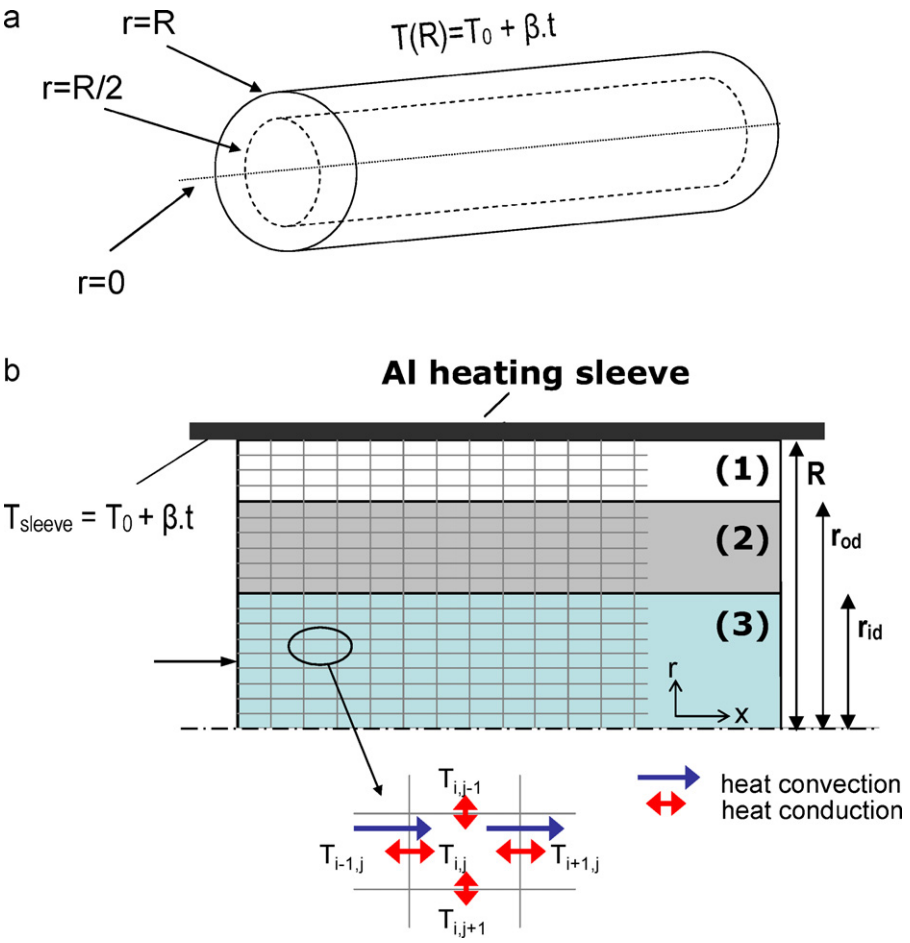

Fig. 1. (a) Schematic drawing of infinitely long cylinder model (simplified model). (b) Schematic layout consisting of the detailed three layer-model ((1) air/thermal paste; (2) silica; (3) open tube/packed column) with finite length. The arrows indicate how the heat is transferred by convection (blue arrows, axial) and by conduction (red arrows, axial and radial). (For interpretation of the references to color in this figure legend, the reader is referred to the web version of the article.)

and velocity, the unretained velocity profile $u_0(r)$ can be directly calculated from the known viscosity profile [53]:

$$u_0(r) = u_{0,\text{wall}} \frac{\eta_{\text{wall}}}{\eta(r)} \tag{3}$$

wherein $u_{0,\text{wall}}$ is the unretained velocity near the wall of the liquid and η_{wall} is the viscosity corresponding to T_{wall}.

The dependency of the retention coefficient on temperature is given by the Van't Hoff equation [5,6]:

$$Ln(k(r)) = \frac{\Delta H_R}{R_g T} + \frac{\Delta S_R}{R_g} + Ln(\phi) \tag{4}$$

wherein k is the retention coefficient, ΔH_R and ΔS_R are the retention enthalpy and entropy, ϕ is the mobile phase fraction and R_g is the universal gas constant. Considering the retention entropy independent of temperature, Eq. (4) can be rewritten and the velocity profile of a retained component u_R can be calculated:

$$k(T(r)) = k_w \exp\left(\frac{\Delta H_R}{R_g}\left(\frac{1}{T(r)} - \frac{1}{T_{\text{wall}}}\right)\right) \tag{5}$$

$$u_R(r) = \frac{u_0(r)}{1 + k(r)} \tag{6}$$

k_w is the retention factor at the capillary's wall ($T = T_{\text{wall}}$). Substituting Eqs. (3) and (5) into Eq. (6), the velocity profile is known and the long-time limit plate height contribution H_{extra} can be calculated using the Aris–Taylor method [14,46,54]:

$$H_{\text{extra}} = \frac{2}{\kappa} \frac{(\Delta u_{\text{Rm}})^2}{u_{\text{Rw}} - \Delta u_{\text{Rm}}} \frac{r_{\text{id}}^2}{D_{\text{rad}}} \tag{7}$$

wherein Δu_{Rm} is the difference between the mean velocity u_{Rm} and the velocity near the column wall u_{Rw} ($\Delta u_{\text{Rm}} = \int_0^1 [u_R(y) - u_{\text{Rw}}]\, 2y\, dy$ and $y = r/r_{\text{id}}$), κ is the geometrical Aris constant, D_{rad} is the radial diffusion coefficient (in the present study the value 10^{-10} m^2/s was used) and r_{id} is the inner radius of the capillary/column. We refer the reader to [14,54] for a detailed explanation on the calculation of Δu_{Rm} and κ.

3. Experimental and numerical methods

3.1. Experimental methods and materials

Measurements were made with two fused silica capillaries (purchased from Optronis GmbH, Kehl, Germany) with an internal diameter of 300 and 530 μm and an outer diameter of 665 and 680 μm, respectively. The length of these capillaries was 20 cm and thereby exceeding the length of the aluminium heating sleeve such that external tubing could easily be connected to the capillary. Measurements were both made with open tube capillaries and packed capillaries, which were slurry packed with fully porous 10 μm Si-particles (Merck LiChrosorb, purchased from Merck KGaA, Darmstadt, Germany). The particles were suspended in a 50/50 vol.% chloroform/iso-propanol solution and packed at

Table 1
Physical and thermal properties of the materials and solvents used in the LTMLC-setup [55,56,65]. The calculations of the packed bed properties are described in Section 4.1.4.

	ρ (kg/m^3)	C_p (J/kg K)	λ (W/m K)	$C_{p,v}$ ($\times 10^{-3}$ J/m^3 K)	α ($\times 10^7$ m^2/s)
Fused Si	2196	703	1.48	1544	9.59
Air	1.164	1007	0.026	1.172	221.81
Thermal paste	2600	1530	10.0	3978	25.14
Open tube					
H_2O	997.0	4180	0.606	4167	1.45
ACN	785.7	2229	0.188	1751	1.07
MeOH	791.4	2531	0.202	2003	1.01
Packed bed, $D = 0.263$, $\varepsilon = 0.40$, $d_p = 10$ μm, $u_{PB} = 5.68 \times 10^{-4}$ m^2/s					
H_2O	1917	1511	0.874	2897	3.02
ACN	1924	997	0.467	1918	2.44
MeOH	1924	1057	0.483	2034	2.38

a pressure of 300 bars. The capillaries were mounted in an aluminium sleeve which could be resistively heated. The temperature ramp of the sleeve was controlled by the capillary column temperature control module LTM A68 (RVM Scientific, Santa Barbara, CA). More details and specifications on this module can be found in [23,41,42]. The aluminium sleeve itself was insulated from the environment with thermal insulation fiber. The heating sleeve had a length of 15 cm and an inner diameter of 790 μm, leading to an air gap between the inner surface of the heating sleeve and the outer surface of the capillary. To study the enhancement in the heat transfer across this air gap, it was filled up with thermal grease Keratherm® KP92 (Kerafol, Eschenbach, Germany). The thermal paste had a thermal conductivity of 10.0 W/m K, a density of 2600 kg/m^3 and a heat capacity of 1530 J/kg K was reported for silicon-based thermal paste [55,56].

An Agilent Capillary LC 1100 system (Agilent Technologies, Waldbronn, Germany) was used to pump HPLC grade water, prepared using a Milli-Q gradient (Millipore, Bedfast, MA, USA) water purification system and stored at room temperature. Flow rates were ranging between 1 and 20 μl/min.

Temperatures were measured with sub-miniature chromel/alumel thermocouples with a diameter of 250 μm (type K, part no. B200, ThermoElectric, Waddinxveen, The Netherlands). The average liquid temperature inside the capillary was measured by inserting the thermocouple in the capillary, far enough to ensure that the thermocouple was positioned in a region where the heating sleeve surrounded the capillary and where the effects of the end zone of the heating sleeve were negligible. The temperature of the aluminium sleeve was measured by placing a thermocouple between the aluminium sleeve and the thermal insulation. The thermocouples were connected to a 24-bit NI 9211 thermocouple input module (National Instruments, Zaventem, Belgium) and the temperature signals were read-out using NI LabVIEW SignalExpress at a frequency of 2 Hz. The thermocouples were calibrated at 25, 50, 75 and 100 °C using a GC-oven (Agilent Technologies, Waldbronn, Germany).

All programmed temperature profiles applied by the LTM heating module consisted of the following subsequent segments: an isothermal segment of 1 min at 30 °C, heating up at 1, 2, 5 or 10 K/s up to 90 °C. The setup is then kept isothermal at 90 °C for 5 min and cooled down to 30 °C by natural convection. This temperature profile has been repeated three times per measurement. The measured data from these individual repeats was shifted in time to align the starting points so that a maximal correlation between all three repeats is obtained, after which the three repeats were averaged out. The measured temperatures from the three repeats had an average RSD $\ll$ 1% and the three measurements had a maximal RSD during the heating segment of 1% for low temperature ramps (1 K/s) and 10% for high temperature ramps (10 K/s), showing the more delicate heating control at high temperature ramps.

3.2. Numerical model and validation of the employed numerical solution methods

To account for the effects that may be missed by the infinitely long cylinder model presented in Fig. 1a and Section 2.1, a more detailed model of the current LTMLC-setup has been built and numerical calculation procedures have been used to investigate its heat transfer properties. The model is shown in Fig. 1b and still constitutes a simplification of the reality, for example because the air layer surrounding the capillary is assumed to be axi-symmetric, whereas this is clearly not the case in reality. The model has however been kept axi-symmetric to keep the computational effort within practically reasonable limits. Fig. 1b, also showing the adopted discretization scheme, represents the LTMLC-setup as an axi-symmetrical annular structure, consisting of three layers: an air layer between the heating sleeve and the capillary, the wall of the capillary (silica layer) and the liquid layer (open tube or packed bed) inside the capillary. The aluminium heating sleeve is reduced to only one row of cells (merely used to impose the applied temperature ramp), because the outer surface of the aluminium sleeve is resistively heated and it is reasonable to assume that only very small temperature gradients will be formed between the outer and inner surface of the heating sleeve. Also the heat loss to the environment is minimized by insulating the outer surface of the heating sleeve.

The heat transfer equation given by Eqs. (8) and (9), shows the different contributions of heat storage, heat convection and axial and radial heat conduction in an infinitesimal thin cylinder layer:

$$\frac{\partial T}{\partial t} = -u(r)\frac{\partial T}{\partial x} + \frac{\lambda_{ax}}{C_{p,v}}\frac{\partial^2 T}{\partial x^2} + \frac{\lambda_{rad}}{C_{p,v}}\left(\frac{\partial^2 T}{\partial r^2} + \frac{1}{r}\frac{\partial T}{\partial r}\right) \tag{8}$$

or in the discretized form, using the same indexing as in Fig. 1b:

$$\frac{dT_{i,j}}{dt} = u(r)(T_{i-1,j} - T_{i+1,j})\frac{A_{ax}}{V_{cell}} + \frac{\lambda_{ax}}{C_{p,v}}\frac{A_{ax}}{V_{cell}}\frac{(T_{i-1,j} - 2T_{i,j} + T_{i+1,j})}{dx} + \frac{\lambda_{rad}}{C_{p,v}}\frac{A_{rad}}{V_{cell}}\frac{(T_{i,j-1} - 2T_{i,j} + T_{i,j+1})}{dr} \tag{9}$$

wherein $u(r)$ is the trans-column velocity profile (parabolic for a flow through an open tube and flat for a flow through a packed column). In the air and silica layer no flow occurs, and the convection term can be discarded there. A_{ax} and A_{rad} are the axial and radial surfaces of the cell with a cell volume V_{cell}. $C_{p,v}$ is the volumetric heat capacity of the material in question (air, silica or liquid) and λ_{ax} and λ_{rad} are the heat conduction coefficients of the material in the axial and radial direction. In the present study, all media were assumed to be isotropic. The values of the physical parameters used in the simulations can be found in Table 1.

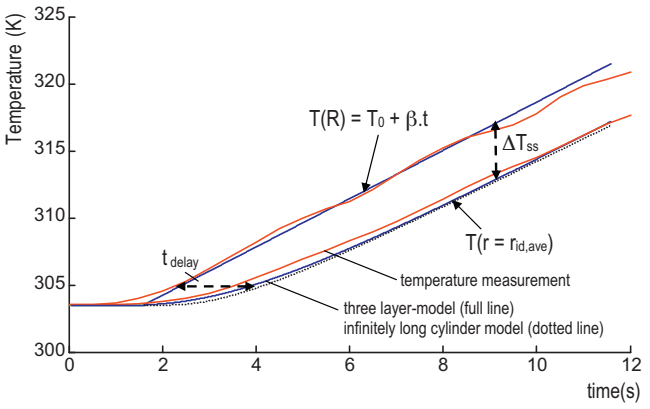

Fig. 2. Experimentally measured thermal response of the LTMLC-system at a heating rate of 1.7 K/s, capillary i.d. 300 μm, o.d. 665 μm and water as solvent at a flow rate of 3 μL/min. In overlay, the data from the infinitely long cylinder model (dotted line) and the detailed three layer-model (full line) are plotted.

The following boundary conditions were employed:

$$\text{Axi-symmetrical axis}: \left.\frac{\partial T}{\partial r}\right|_{r=0} = 0 \tag{10}$$

Adiabatic walls at the beginning and the end of the capillary:

$$\left.\frac{\partial T}{\partial x}\right|_{x=0} = 0 \quad \text{and} \quad \left.\frac{\partial T}{\partial x}\right|_{x=L_{cap}} = 0 \tag{11}$$

$$\text{Non pre-heated mobile phase temperature}: T = T_0 \tag{12}$$

$$\text{Pre-heated mobile phase temperature}: T = T_0 + \beta t \tag{13}$$

The discretized heat transfer equations were numerically solved using a 4th order Runge–Kutta scheme [45]. The cells have a length *dx* of 20 μm (axial size) and a height *dr* of 5 μm for the liquid and silica layer and a height *dr* of 10 μm for the air layer (radial size). The finite time step *dt* was taken 2×10^{-7} s. The number of cells in the axial direction is 101 and the number of cells in the radial direction corresponds with the capillary's geometry (69 and 71 cells for the capillary with outer diameter 665 and 680 μm respectively). The average temperature of the outflowing liquid was determined using the following equation:

$$T_{liq,ave} = \frac{2}{r_{id}^2}\int_0^{r_{id}} T(r) r dr \tag{14}$$

where r_{id} is the radius of the liquid layer (the inner radius of the capillary).

The analytical solution (Section 2.1) was used to validate the results from the numerical model. For this purpose, a cylinder of silica (radius of 250 μm, $\beta = 1$ K/s, no flow) was simulated with the above numerical model. A maximal error on $T_{(r=R)} - T_{(r=0)}$ of 2% existed between the analytical and the numerical result. This error is acceptable, given the large degree of simplification in the numerical model compared to the real LTMLC-setup.

4. Results and discussion

4.1. Heat transfer in the LTMLC-system: temperature measurements and simulations

The thermal response of the LTMLC-system is shown in Fig. 2 for an open-tubular fused-silica capillary (i.d. 300 μm and o.d. 665 μm), taking water as the mobile phase ($F = 3$ μL/min) and for a temperature ramp of $\beta = 1.7$ K/s. The figure shows the difference between the measured temperature of the heating sleeve (indicated by $T(R)$) and the measured average liquid temperature (indicated by $T(r = r_{id,ave})$), as well as the analytical solution of the temperature distribution discussed in Section 2.1 (dotted line) and the numerical results from the more detailed model discussed in Section 3.2 (full line).

Fig. 2 shows that there is a certain delay (indicated by t_{delay}-arrow) at the start of the temperature ramp between the temperature increase of the liquid layer and the imposed temperature increase at the heating sleeve. During this transient regime, the setup is heated up but insufficient heat is transferred to the liquid layer, leading to a continuously increasing difference between the liquid temperature and the temperature of the heating sleeve. After a certain time (further referred to as the lag time t_{lag}), the thermal steady-state regime takes place wherein the whole LTMLC setup including the liquid inside the capillary is heated up at the same temperature ramp (β) as the heating sleeve, but with a given temperature offset ΔT_{ss} as indicated by the arrow on Fig. 2. The analytical expression of ΔT_{ss} can be derived from Eq. (1), because this reduces in the long-time limit to:

$$\lim_{t\to\infty} \Delta T(r) = \Delta T_{ss}(r) = (T_0 + \beta t) - \lim_{t\to\infty} T(r) = \beta \frac{R^2 - r^2}{4\alpha} \tag{15}$$

Subsequently integrating this difference across the cross-sectional area accessible to the liquid (because the thermocouple measures the average liquid temperature), the following expression is obtained for the temperature difference between the heated outer wall and the liquid in the interior of the capillary:

$$\Delta T_{ss} = \beta \frac{R^2 - 1/2 r_{id}^2}{4\alpha_{lumped}} \tag{16}$$

This expression shows that, according to the simplified infinitely long cylinder model, the constant temperature offset can be expected to depend linearly on the temperature ramp, quadratically on the cylinder's radius and inversely on the thermal diffusivity α. The expressions also shows that a high heat conductivity and a low thermal mass increase the thermal diffusivity and will thus decrease $\Delta T_{ss}(r)$. In the following sections, these predictions will be compared with the experimental measurements.

To magnify the view on the temperature difference, the experimentally obtained temperature responses are represented as the temperature difference between the heating sleeve and the liquid, rather than as the absolute temperature as was done in Fig. 2. Fig. 3 shows such a temperature difference plots for different temperature ramps. The reader will note that the $\beta = 1.7$ K/s-curve shown in Fig. 3a is the ΔT-representation of the liquid phase temperature curve already shown in Fig. 2. In all represented cases in Fig. 3, both the measured and the simulated temperature responses display a clear transient range, followed by a steady-state thermal offset range. As can be noted, the steady-state thermal offset regime is in the presently considered set-up always reached after approximately 7 s, independently of the heating rate (see t_{lag}-indication on Fig. 3a). The simplified infinitely long cylinder model provides an analytical expression for this lag time, defined here as the time needed to reach, e.g., 99% of the thermal offset value ΔT_{ss}. Starting from Eq. (1), and making the approximation that the second and higher terms of the summation in Eq. (1) can be discarded (valid since $\zeta_2^3 J_1(\zeta_2) \gg \zeta_1^3 J_1(\zeta_1)$), the following expression for the lag time is obtained:

$$t_{lag}(99\%\ \text{of}\ \Delta T_{ss}) = \frac{Ln(0.01) R^2}{-\alpha (2.405)^2} \tag{17}$$

wherein $2.405 = \zeta_1$, the 1st root of $J_0(\zeta_1) = 0$. Eq. (17) shows that the time needed to reach the thermal steady state is only dependent on the geometry of the setup (via R) and on the total 'lumped' heat transfer parameter α, but is independent of the heating rate. The latter is in agreement with the observation that can be made from the experiments shown in Fig. 3.

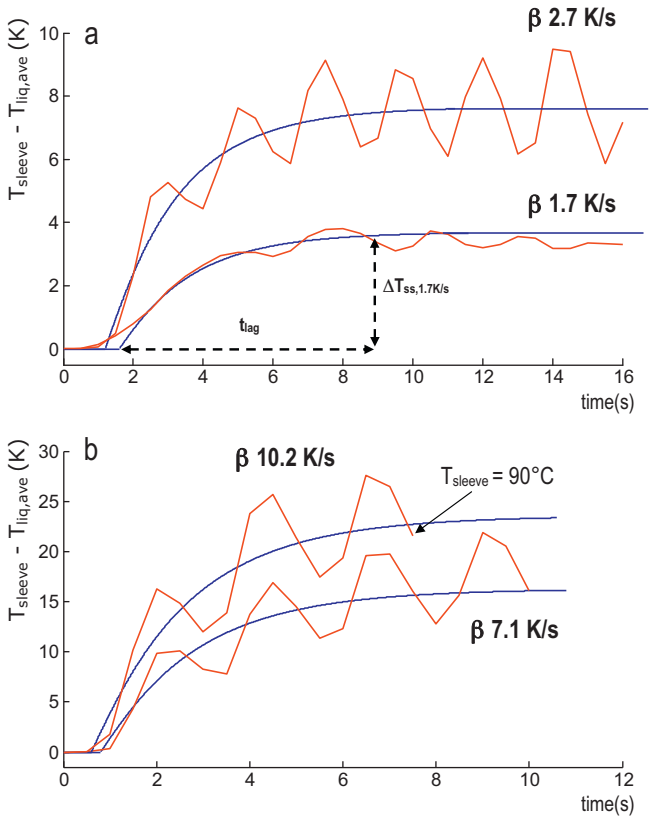

Fig. 3. Experimentally measured (red line) and simulated (blue line) temperature difference between the heated wall and the liquid for heating rates of (a) 1.7 K/s and 2.7 K/s and (b) 7.1 K/s and 10.2 K/s respectively. Capillary i.d. 300 μm, o.d. 665 μm. The capillary is used as open tube, the solvent is water at a flow rate of 3 μL/min. (For interpretation of the references to color in this figure legend, the reader is referred to the web version of the article.)

Also in agreement with the theoretical expectations based on Eqs. (15) and (16), is that the temperature offset scales linearly with the heating rate. This was qualitatively confirmed by the measurements: ΔT_{ss} respectively increases with a factor 2.1 and 4.5 when β increases with a factor 1.6 and 4.2. For very high temperature ramps, the steady-state regime is not reached (see for example the case shown in Fig. 3b), because the end-temperature of the cycle (90 °C in the present study) was already reached in about 6 s at 10.2 K/s, falling within the time to reach the steady-state thermal offset regime. At the end of the applied temperature ramp, thus when the end-temperature is reached and the heating sleeve is kept isothermal, the temperature difference between the heating sleeve and the liquid tends to zero again and the temperature of the liquid shows a thermal response that is inverse to the transient response at the start of the temperature ramp (data not shown).

Fig. 2 also shows good overlap between the measured thermal response and the simulated or calculated temperature data. Whereas the analytical expression is only a very simplified model of the LTMLC-system and uses a 'lumped' heat transfer coefficient, the more detailed numerical model employs the thermal properties of the three material layers present in the LTMLC-system and can be used to investigate the impact of these three layers in the setup. In the numerical scheme shown in Fig. 1b, the setup was assumed to be axi-symmetrical but in practice, the heating sleeve rests on the capillary, making contact with the top side of the capillary and leaving a larger gap at the bottom side. To account for this issue, the thickness of the air gap was reduced to 25 μm (instead of 62.5 μm) such that the numerical results corresponded well to the measured average temperature for the four different considered heating rates.

Considering that the infinitely long cylinder solution is a model wherein no axial temperature gradients occur, and considering that this model already provides a good approximation to the measured temperature response (cf. Fig. 2), it can be concluded that the LTMLC-system displays no significant axial temperature gradients. This might seem in contradiction with the fact that the experiments were conducted without mobile phase pre-heater, so that one would expect the formation of an axial temperature gradient at the capillary inlet (thermal inlet region) where the incoming liquid is heated up by the first section of the heated silica capillary. However, it can be calculated that this inlet length is relatively small compared to the total capillary length, so that the axial gradient in the inlet region can indeed be neglected. Using the procedures described in [6,57], it can be calculated that for a capillary with the same dimensions as used in the present study (i.d. 300 and 530 μm; o.d. 665 and 680 μm respectively), the length needed to heat up the incoming liquid from 30 to 89.9 °C (1% offset from T_{max} = 90 °C) is smaller than 1 mm for conventional capillary LC flow rates (1–5 μL/min) and thus showing that the thermal impact of not pre-heating the mobile phase is negligible for the common capillary LC columns and conditions. In the numerical simulations conducted with the finite, three-layer model shown in Fig. 1b, the entrance can no longer be neglected (since the numerical model was only 2 mm long) and the boundary condition of a pre-heated mobile phase was used in the numerical model (cf. Eq. (13)).

Fig. 3 also shows that the measured temperature signal displays a strong, periodic fluctuation. These are due to the non-perfect controlling of the temperature ramp. The amplitude of the fluctuations varies according to the heating rate, and where the fluctuations are only 1 K in amplitude for the measurement at β = 1.7 K/s, they increase up to 10 K for a heating rate of β = 10.2 K/s. The thermal offset values are thus given by $\Delta T_{ss} = 3.6 \pm 0.5$ and 22.4 ± 5 °C for heating rates of β = 1.7 and 10.2 K/s, showing that the contribution of the fluctuations to the thermal offset is a moderate but acceptable 20%.

4.1.1. *Effect of the capillary dimensions and mobile phase*

Comparable results are shown in Fig. 4 for a wider capillary, i.e., one with an i.d. of 530 μm and an o.d. of 680 μm. The same conclusions can be drawn as in Fig. 3: the transient thermal response, being independent on the heating rate, is again followed by a thermal steady-state which scales linearly with the heating rate. Comparing with the results from Fig. 3, it can be noted that the transient lag time is longer (9 s vs. 7 s) and that the thermal offset is higher (5.5 K vs. 3.6 K, β = 1.8 K/s). Due to the larger inner diameter of the capillary, the ratio H_2O/Si of the setup is increased, leading to a decrease of the 'lumped' thermal conductivity and an increase in total thermal mass, which results in an overall increase of the total resistance to heat transfer for the capillary dimensions used in Fig. 4 compared to Fig. 3.

In addition to this, the mobile phase has a lower velocity (Fig. 4 vs. Fig. 3) since the flow rate in both capillaries was kept constant, leading to a slight reduction of the heat transfer. However, in Section 4.1.2, it is shown that this only marginally contributes to the larger thermal offset.

Similar temperature profiles would be measured for methanol or acetonitrile as solvent. Both the thermal conductivity and the thermal mass of methanol and acetonitrile are lower compared to water (see Table 1 for the physical and thermal properties of the common LC solvents), leading to more or less comparable thermal diffusivity: α = 1.45, 1.01 and 1.07 × 10^{-7} m^2/s for respectively water, methanol and acetonitrile. Numerical calculations with the three-layer model predict for a temperature ramp of 1.7 K/s a temperature offset of 3.8 K for a capillary with an i.d. 300 μm and o.d. 665 μm and 4.5 K for the capillary with an i.d. 530 μm and o.d. 680 μm for the case of methanol. For acetonitrile, the temperature

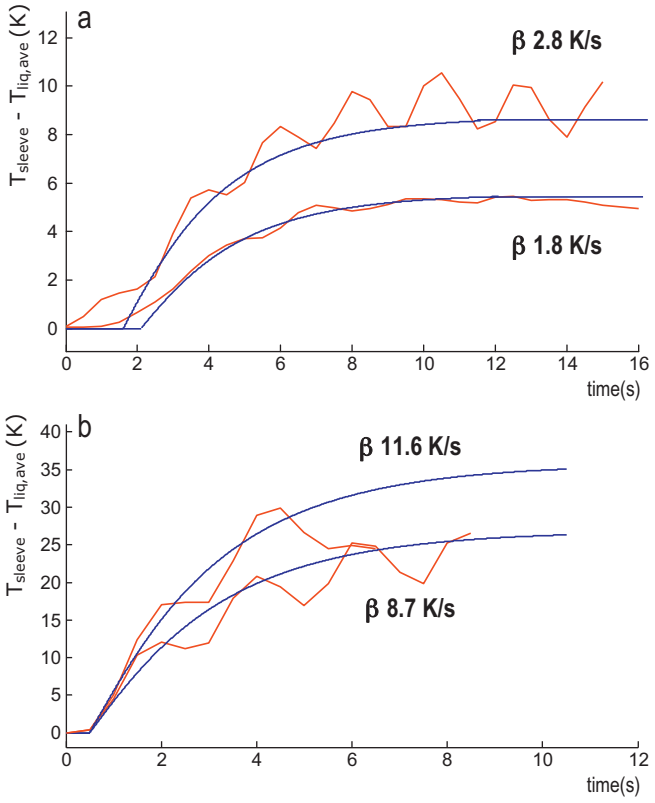

Fig. 4. Experimentally measured (red line) and simulated (blue line) temperature difference between the heated wall and the liquid for heating rates of (a) 1.8 K/s and 2.8 K/s and (b) 8.7 K/s and 11.6 K/s respectively. Capillary i.d. 530 μm, o.d. 680 μm. The capillary is used as open tube, the solvent is water at a flow rate of 3 μL/min. (For interpretation of the references to color in this figure legend, the reader is referred to the web version of the article.)

offset is 3.7 K and 4.4 K respectively. Since the thermal conductivity, the density and the heat capacity of binary liquid mixtures can be approximated by the average of the properties of its single components (average weighted by the mass fractions), no big change in thermal diffusivity can be expected during a methanol/water or acetonitrile/water mobile phase gradient and one can hence expect only a slightly increasing value of the thermal offset ΔT_{ss} during the gradient, depending on the inner diameter of the capillary.

4.1.2. Effect of the mobile phase velocity

The temperature response in Figs. 3 and 4 was measured for a flow rate of 3 μL/min. The heat transfer can be improved by increasing the flow rate as shown in Fig. 5 (capillary i.d. 530 μm and o.d. 680 μm). For a flow rate of 20 μL/min, a steady-state thermal offset value of 3.2 K was measured and a corresponding lag time of 6.5 s, which is an improvement of 40% compared to the data shown in Fig. 4 for a temperature ramp of 1.8 K/s (F = 3 μL/min: ΔT_{ss} = 5.5 K and t_{lag} = 9 s). For flow rates between 1 and 5 μL/min, which are conventional flow rates for the capillary dimensions used in the present study, the difference in thermal offset value ΔT_{ss} is only 1 K, falling within the amplitude of the fluctuations which are caused by the non-perfect controlling of the temperature at low temperature ramps. Fig. 5 also shows that for no flow of the mobile phase (dashed curve on Fig. 5), as is the case in the analytical solution elaborated in Section 2.1, the highest thermal offset can be expected. Simulation results show a thermal offset value of ΔT_{ss} = 5.8 K and a corresponding lag time of t_{lag} = 9.5 s, lying closely to the measured thermal offset and lag time for a flow rate of 3 μL/min (ΔT_{ss} = 5.5 K and t_{lag} = 9 s). Because of the higher mobile phase velocity, the heat transfer by axial convection in the liquid layer increases (see Fig. 1b

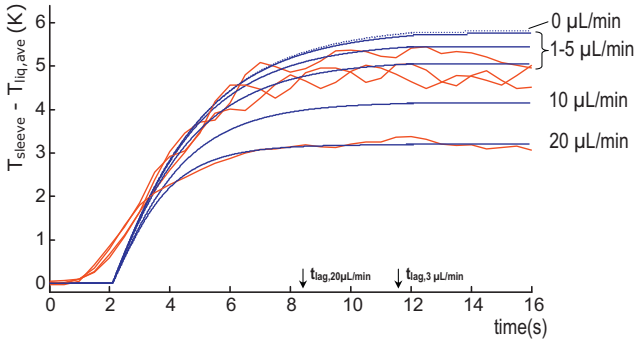

Fig. 5. Experimentally measured (red line) and simulated (blue line) temperature difference between the heated wall and the liquid for flow rates of 1, 3, 5, 10 and 20 μL/min (ordered in descending thermal offset). Capillary i.d. 530 μm, o.d. 680 μm. The capillary is used as open tube with water as solvent. The temperature ramp is 1.8 K/s for the flow rates between 1 and 5 μL/min and 1.6 K/s for 10 and 20 μL/min. (For interpretation of the references to color in this figure legend, the reader is referred to the web version of the article.)

and Eqs. (8) and (9)), leading to an overall decrease of the heat transfer resistance.

4.1.3. Effect of the air gap and the use of thermal paste

Due to the construction of the LTMLC-system, where a capillary is slid in a heating sleeve, an air gap is inevitably formed between the outer surface of the capillary and the inner surface of the heating sleeve. The impact of the thickness of the air layer on the thermal performance of the LTMLC-system is shown in Fig. 6a, where the

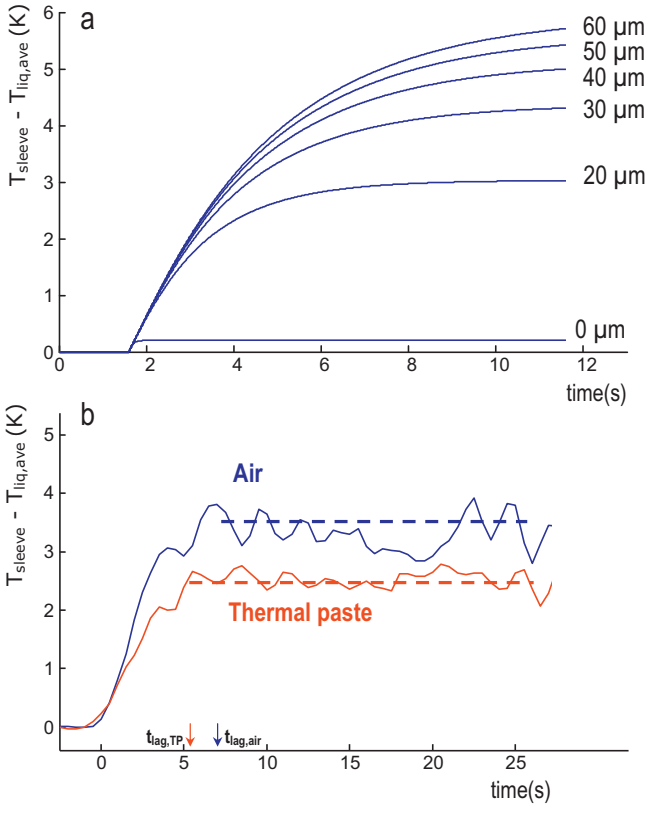

Fig. 6. Temperature difference between wall and out flowing liquid, showing (a) the influence of the thickness of the air layer and (b) the influence of thermal paste (blue: air layer; red: thermal paste layer). Conditions: capillary i.d. 300 μm, o.d. 665 μm, β = 1.7 K/s, F = 3 μL/min. The dashed line indicates the average steady state thermal offset. (For interpretation of the references to color in this figure legend, the reader is referred to the web version of the article.)

simulated temperature profiles are shown for various values of the air layer thickness, ranging between 20 and 60 μm (same conditions and capillary dimensions as in Fig. 3). As can be noted both the steady-state thermal offset and the lag time increase strongly with increasing air layer thickness. For an air layer thickness of 40 μm, the lag time is $t_{lag} \approx 10$ s, much larger than the lag time of 7 s measured for an air layer of 25 μm and equivalently the thermal offset of $\Delta T_{ss} = 5.0$ K for a thickness of 40 μm is larger than the 3.6 K measured for a thickness of 25 μm.

Fig. 6a shows how sensitive the thermal response of the LTMLC-system is to the air gap between the capillary and the heating sleeve. In the ideal situation, when no air layer exists, as is the case when the outer diameter of the capillary equals the inner diameter of the heating sleeve, a thermal offset value of $\Delta T_{ss} = 0.2$ K would be obtained in a lag time of $t_{lag} = 0.4$ s. Even a slight air gap (20 μm, Fig. 6a), which is in practice anyhow difficult to avoid, already decreases the thermal performance of the LTMLC-setup. A possible way to circumvent the problematic heat transfer across the air layer is to fill up the air gap with thermal paste which has a very high thermal conductivity, but also a higher thermal mass. The measured temperature profile is shown in Fig. 6b for a capillary with and without thermal paste. An improvement of 1 K can be noted ($\Delta T_{ss,TP} = 2.5$ K and $\Delta T_{ss,air} = 3.6$ K), but the minimal thermal offset value (in the case of no air layer) is not reached because it is difficult to apply the thermal paste homogeneously and without the formation of air voids which lead to a reduced heat transfer. More importantly, the thermal paste also induces a small but non-negligible resistance to heat transfer and because the thermal paste surrounds the capillary completely, the distance from the capillary's outer surface to the inner surface of the heating sleeve is 62.5 μm on both sides, whereas for the case of the air layer, the capillary rests on the heating sleeve and an equivalent air layer thickness of 25 μm was found.

The disadvantage of the thermal paste is its high thermal mass. For fast temperature cycles or temperature pulses, it is hence more advisable to minimize the thermal mass as much as possible and use the setup with the air layer instead of the thermal paste. On the contrary, when a good temperature control of the liquid temperature is wanted, the thermal paste should be inserted to minimize the thermal offset and the lag time. Another advantage of the thermal paste is the smaller amplitude of the fluctuations in the measured temperature signal, as can clearly be noted from Fig. 6b. The smaller sensitivity to temperature fluctuations of the thermal paste system is due to its higher thermal mass.

Additionally, the thermal lag time might also be undesired when a good temperature control of the liquid is wanted, because during the lag time, the mobile phase is heated up at a lower temperature ramp than the heating sleeve (cf. Fig. 2). When the lag time is not excessive (small capillaries) and when only low temperature ramps are applied, the thermal time lag can be circumvented by a delayed injection. Instead of synchronising the injection and the start of the temperature ramp, which goes, e.g., from 30 °C to 90 °C at a temperature ramp of 1 K/s, the injection is now made 10 s later than the start of temperature program which runs from 20 °C to 90 °C. The injected molecules will still perceive the original temperature program but the thermal time lag has been omitted (assuming that $t_{lag} < 10$ s) and the same temperature ramp as the heating sleeve is already observed in the liquid layer at the moment of injection.

4.1.4. Effect of packing

Whereas the data shown in Figs. 2–6 only relate to open-tubular columns, most capillary LC applications use packed capillaries, filled with either particles or monoliths [58]. Fig. 7 compares the temperature response between a capillary packed with 10 μm bare silica particles with that of an open-tubular capillary. Both capillaries had an i.d. of 530 μm and an o.d. of 680 μm and in both cases, the

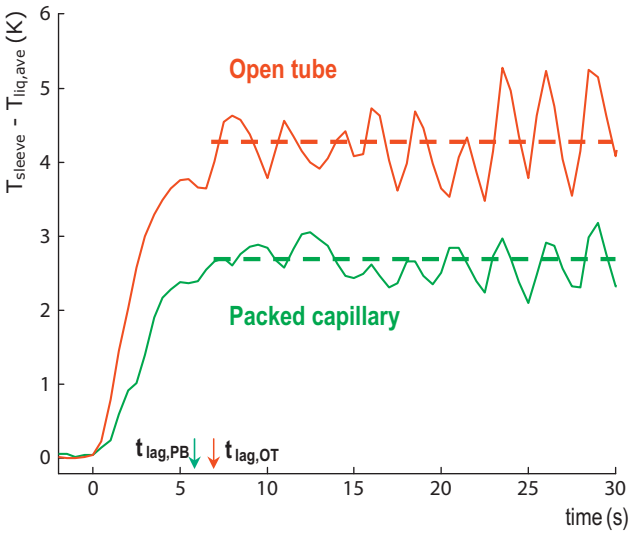

Fig. 7. Measured temperature difference between wall and out flowing liquid for an open tube (red) and a capillary packed with 10 μm silica particles (green). Conditions: capillary i.d. 530 μm, o.d. 680 μm, thermal grease, $\beta = 1.8$ K/s, $F = 3$ μL/min. The dashed line indicates the average steady state thermal offset. (For interpretation of the references to color in this figure legend, the reader is referred to the web version of the article.)

air gap was filled with thermal paste. As can be noted, the presence of the silica particles reduces the thermal offset value from 4.3 K to 2.7 K, while also the lag time reduces from 7 to 6 s.

The main reason for the improved thermal response of the packed capillary is to be found in the increased thermal conductivity of the medium filling the capillary. The effective thermal conductivity of a heterogeneous packed bed (λ_{PB}) composed of porous particles impregnated with the mobile phase, can be described with a two-component system as was proposed by Zarichnyak and Novikov under no-flow conditions [59]:

$$\lambda_{PB}(u_{PB} = 0) = \varepsilon^2 \lambda_{Si} + (1-\varepsilon)^2 \lambda_{H_2O} + 4\varepsilon(1-\varepsilon)\frac{\lambda_{Si}\,\lambda_{H_2O}}{\lambda_{Si} + \lambda_{H_2O}} \quad (18)$$

For a porosity of $\varepsilon = 0.40$ and water as mobile phase liquid, the packed bed has a thermal conductivity of 0.868 W/m K, which is an increase of 43% compared to the pure mobile phase for an open tube capillary under no-flow conditions. Similar results can be obtained for acetonitrile or methanol as mobile phase. However, for a packed bed, the velocity profile is not parabolic but is macroscopically described as a plug flow, i.e., a constant average velocity over almost the complete cross-section of the capillary, but steeply decreasing to zero at the inner surface of the capillary to preserve the no-slip condition. When investigating the flow in a packed bed on a microscopic scale, Eddy dispersion will be observed due to the heterogeneous character of the packing structure and the local mixing of different flow paths will increase the radial heat convection (similar to radial dispersion in packed beds). The effective thermal conductivity of the packed bed with a non-zero mobile phase velocity can be calculated by [60]:

$$\lambda_{PB} = \lambda_{PB}(u_{PB} = 0) + D u_{PB} d_p C_{p,H_2O} \quad (19)$$

D is a constant related to the radial dispersion coefficient ($D u_{PB} d_p$) and depends on the particle diameter. Extrapolating the measurements from both Knox and Tallarek ($D = 0.064$ for 64 μm particles and $D = 0.3$ for 5 μm particles [61,62]), a value of 0.263 was estimated for the case of 10 μm particles, assuming a linear relation between $\log(D)$ and d_p [60]. An effective thermal conductivity of 0.874 W/m K was calculated for water as mobile phase, 10 μm particles, a flow rate of 3 μL/min ($u_{PB} = 5.68 \times 10^{-4}$ m/s) and a bed porosity of $\varepsilon = 0.40$. Comparing the static and dynamic thermal con-

ductivity of the packed bed, it can be noted that the contribution of the radial dispersion is very small (<1%) for the system under investigation. Table 1 shows similar results for acetonitrile and methanol as mobile phase. Also the density and heat capacity of the packed bed is shown in Table 1, calculated by the averaged properties of the pure mobile phase liquid and silica (weighted by the mass fractions). The thermal mass of the packed bed is also lower than that of the corresponding liquid in an open tube, resulting in an overall decrease of the thermal diffusivity and (mainly) explaining the improved heat transfer shown in Fig. 7.

4.2. Band broadening in the LTMLC-system

Because the temperature implied on the heating sleeve of the LTMLC-system ($T_{sleeve} = T_0 + \beta t$) is higher than the temperature inside the setup, radial temperature gradients exist across the LTMLC-setup and thus across the liquid layer resulting in the dispersion of species. In Section 4.1, it was shown that after the thermal lag time of the LTMLC-system, the same temperature ramp is applied to the whole system but with a certain steady-state thermal offset between the wall and the interior of the capillary. It was also shown that the shape and the amplitude of the temperature gradients across each layer of the LTMLC-setup will remain constant in the steady-state regime, even though the temperature inside the liquid layer constantly changes (cf. Fig. 2). As a consequence, the temperature gradients across the different layers will not influence each other and the infinitely long cylinder model will provide a good estimate for the steady-state radial temperature gradient in the liquid layer. Doing so, it should be remarked that Eq. (15) should be modified such that only the temperature gradient across the liquid zone (open tube or packed bed) is taken into account:

$$\Delta T_{liq} = T_{wall,liq} - T_{axis,liq} = \beta \frac{r_{id}^2}{4\alpha} \tag{20}$$

Fig. 8a shows the maximal radial temperature difference values ΔT_{liq} calculated via Eq. (20) for a packed bed capillary filled with either water (full lines), acetonitrile (dash-dotted lines) or methanol (dotted lines) and for different temperature ramps (employed properties of the packed bed are given in Table 1). As can be noted, the ΔT_{liq}-values obtained for acetonitrile lie close to those obtained for methanol because both solvents have approximately the same thermal diffusivity and therefore the same temperature gradients are formed in the liquid layer. In full agreement with Eq. (20), all represented ΔT_{liq}-values show a quadratic dependency on the inner diameter and are linearly proportional with the temperature ramp β. Fig. 8a for example shows that (for the case of water as solvent) a radial temperature difference of 0.9 K is obtained for a narrow-bore column of 2.1 mm for β = 1 K/s, whereas the same ΔT_{liq} = 0.9 K is already achieved with a column diameter of about 660 μm when the temperature ramp is increased to β = 10 K/s (maximal column diameter scales according to square root of R, corresponding to a factor $\sqrt{10}$ in the present case). Similarly, a gradient of ΔT_{liq} = 0.2 K is found for β = 1 K/s in a micro-bore column of 1 mm, whereas a ΔT_{liq} = 2.1 K is found when a temperature ramp of β = 10 K/s would be for the same column (ΔT_{liq} scales linearly with β according to Eq. (15)).

Subsequently taking the ΔT_{liq}-values and using them in Eqs. (2)–(7) to calculate the accompanying expected additional band broadening (represented as an additional plate height contribution H_{extra}), the values shown in Fig. 8b–d are obtained. Fig. 8b compares the case of a packed bed filled with water (full lines) with one filled with methanol (dotted lines). Fig. 8c compares the expected band broadening in water (full lines) with that in acetonitrile (dotted lines). In Fig. 8b and c, the data were calculated for the case of a small molecule with a strong retention enthalpy (ΔH_R = −15 kJ/mol). The effect of the retention enthalpy is represented in Fig. 8d.

The thus obtained relations between H_{extra} and the capillary diameter all display the same trend: for small inner diameters, the expected band broadening is very small and increases only very slowly with r_{id}, whereas the H_{extra}-values steeply increase when a certain critical inner diameter is exceeded. More or less arbitrarily defining the critical inner diameter as the value for which H_{extra} starts to exceed ≈0.3 μm, it can be noted, first from Fig. 8b, that the critical inner diameter depends heavily on the applied temperature ramp β. At high temperature ramps, the critical inner diameter is much smaller compared to lower temperature ramps, as a direct consequence of the increased radial temperature gradients shown in Fig. 8a. Rewriting Eq. (2) shows the influence of ΔT_{liq} on the maximal viscosity difference in the liquid layer:

$$\log_{10}\left(\frac{\eta_{max}}{\eta_{min}}\right) = \frac{B}{T_{wall,liq} - C} - \frac{B}{T_{wall,liq} - \Delta T_{liq} - C} \tag{21}$$

For a large temperature gradient ΔT_{liq}, which is the case when high temperature ramps are applied or large capillary inner diameters are used, the ratio of the maximal to minimal viscosity will be larger, resulting into a larger contribution to band broadening.

The critical capillary inner diameter also depends on the employed mobile phase. The poorer heat transfer in methanol or acetonitrile compared to water (cf. Table 1) leads to some slightly larger radial temperature gradients, as is shown in Fig. 8a. This is partially compensated by the fact that the viscosity of methanol (and also acetonitrile) is less dependent on the temperature compared to water. Although, the coefficient B in the Vogel-equation (cf. Eqs. (2) and (21)) is larger for methanol and acetonitrile compared to water, the coefficient C is much smaller, leading to a lower dependency of the viscosity on the temperature for the organic solvents under consideration.

For methanol (Fig. 8b), the impact of the increased temperature gradient ΔT_{liq} in the liquid layer dominates, leading to a slightly larger band broadening. For the case of acetonitrile (Fig. 8c), the impact of the low dependency of the viscosity on temperature dominates at low temperature ramps (β = 1 K/s) and the contribution to band broadening will be smaller for acetonitrile compared to water. However, at higher temperature ramps (β = 10 K/s), the difference in maximal temperature gradient in the liquid layer for water and acetonitrile becomes very larger and dominates, resulting in a higher contribution to band broadening for acetonitrile as mobile phase. At intermediate temperature ramps (β = 2 K/s), both the water and acetonitrile curve coincide. During a methanol/water gradient, and equivalently an acetonitrile/water gradient, the plate height contribution will vary between the two extreme curves of the pure liquids.

At high temperature ramps (β = 10 K/s), the critical diameter is around 900–1000 μm. At low temperature ramps (β = 1 K/s), narrow-bore packed bed columns (i.d. = 2.1 μm) can be used. This is in agreement with the work of Molander et al. [63], who found no negative influence on the separation efficiency for a 4.6 mm i.d. column, a 50/50 vol.% acetonitrile/water mobile phase when applying a weak temperature ramp of only 20 °C/min (0.33 K/s). Also in previous studies, it was pointed out that the band broadening for higher temperature ramps was reasonable when using columns with micro-scale dimensions [23].

Also the temperature dependence of the retention of molecules is an important parameter in the contribution to the plate height. Fig. 8d shows the plate height increase associated with these radial temperature gradients, for the case of a packed bed column with pure water and considering both a strong and weak dependence of the retention of small molecules on temperature (ΔH_R = −15 and −5 kJ/mol respectively for the full line and the dotted line curve, cf. Eqs. (4) and (5) and Ref. [14]). Obviously, the effect is stronger for molecules with a high retention-temperature dependency (full lines), where a stronger band broadening can be expected because

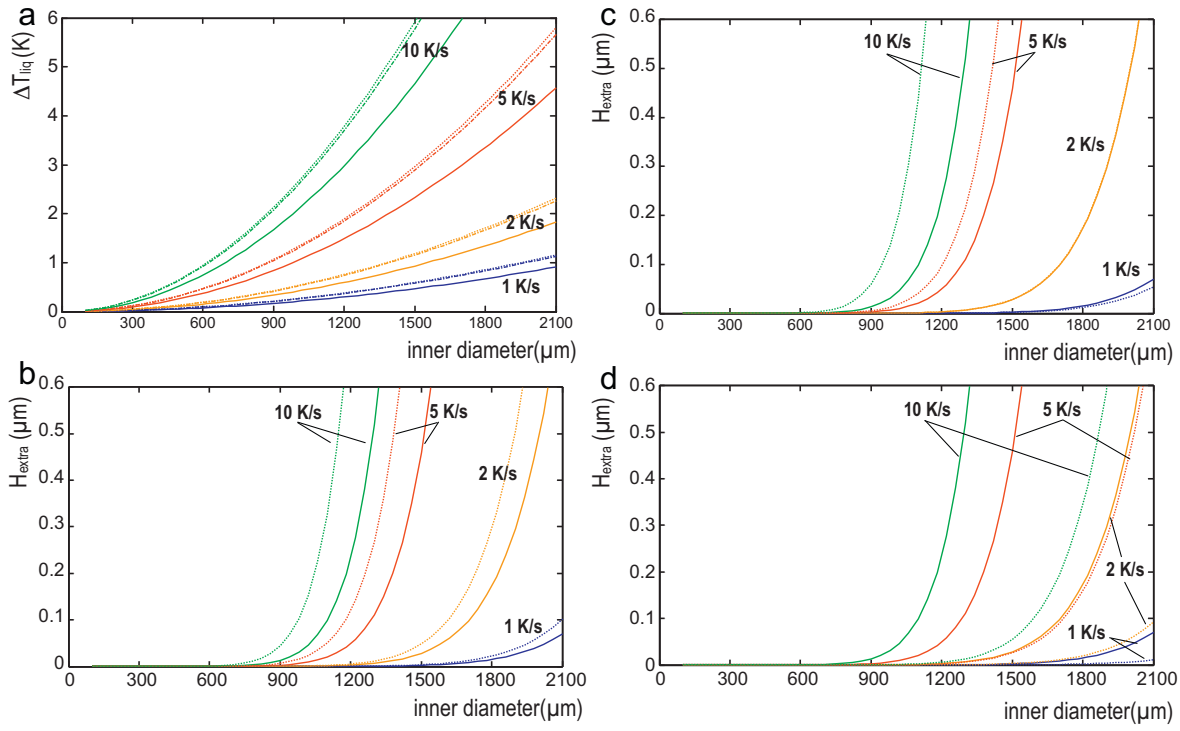

Fig. 8. (a) Maximal radial temperature gradient in the liquid layer (packed bed, no flow) as function of the inner diameter and the temperature ramp for different solvents: water (full lines), methanol (dotted lines) and acetonitrile (dash-dotted lines). (b) Contribution to the band broadening for a retained component (k' = 3 at 30 °C, ΔH_R = −15 kJ/mol, packed bed), comparing water (full lines) and methanol (dotted lines) and (c) water (full lines) and acetonitrile (dotted lines) as mobile phase. (d) Contribution to the band broadening for a retained component (k' = 3 at 30 °C) with a high (full lines) and low (dotted lines) temperature dependency (ΔH_R = −15 and −5 kJ/mol respectively, packed bed, no flow, water).

the radial velocity gradient of the retained species will be larger compared to species with a lower retention-temperature dependency (dotted lines). For macromolecules, even higher retention enthalpies can be expected (absolute values) resulting in an even higher contribution to band broadening [14,64].

A few comments on the above calculated plate height contributions have to be made. First of all, the band broadening will not be constant during the heating segment of the temperature program. In the transient regime (cf. Fig. 2), the temperature gradients in the liquid layer will be smaller than the ΔT_{liq}-values shown in Fig. 8a. Consequently, the plate height contribution will be lower in during the thermal time lag at the beginning of the temperature ramp. In addition, because of the increasing liquid temperature during the temperature program, and because the viscosity is less dependent on temperature at high temperatures, the (retained) velocity gradients will be smaller at higher temperatures (at the end of the temperature ramp). This will further lower the expected band broadening. Comparing for a wall temperature $T_{wall,liq}$ of 90 °C instead of 30 °C as was used in Fig. 8b–d, the H_{extra} values were 82 and 62% smaller for temperature ramps of 1 and 10 K/s, respectively.

A second comment is that when the inner diameter is increased (e.g., to 2.1 mm, which is acceptable for a temperature ramp of β = 1 K/s), it has to be taken into account that for mechanical purposes, a thicker column wall is needed and that the thermal mass of the LTMLC-system will largely increase, resulting in a much larger steady-state thermal offset value ΔT_{ss} and lag time t_{lag}.

5. Conclusions

The heat transfer in the LTMLC-system is investigated with an analytical model (infinitely long cylinder model) which uses a lumped heat transfer parameter, but also with a numerical model (three-layer model) to investigate the contribution of each layer (liquid layer, capillary wall and air layer). Both models were validated by experimental temperature measurements made by placing miniature thermocouples in the LTMLC-system.

It was found that when a certain temperature ramp is applied to the LTMLC-system, that firstly a transient temperature regime is noted during which the heat is transferred from the aluminium heating sleeve to the liquid layer. After this lag time, the entire setup including the liquid layer is then heated up at the same temperature ramp, but with a certain temperature offset between the liquid layer and the temperature of the aluminium heating sleeve. For an open tubular capillary column with an i.d. of 300 μm and an o.d. of 665 μm, a lag time of 7 s and a steady state offset temperature of 3.6 K was found (water, β = 1.8 K/s, F = 3 μL/min). When increasing the capillary inner diameter to 530 μm (and the same o.d. and conditions), the thermal lag time and thermal offset value increased to 9 s and 5.5 K, due to the increased mobile phase/silica ratio. The infinitely long cylinder model gives some simple correlations between the thermal lag time and steady state thermal offset value and the system dimensions and thermal properties. When an appropriate value for α is known, these correlations are sufficiently accurate to predict the main thermal behaviour of the system. These correlations predict that both the thermal lag time and the steady state thermal offset value scale quadratically with the dimensions of the setup (R^2 [m^2]) and are inversely proportional to the 'lumped' thermal diffusivity (α [m^2/s]). The thermal offset also scales linearly with the applied temperature ramp (β [K/s]), whereas the thermal lag time is independent of the temperature ramp.

Upon increasing the flow rate, the thermal lag time and the steady state thermal offset decreased. In the flow rate range typical for the capillaries used in the present work (1–5 μL/min), the gain is about 1 K. Comparing a packed bed with an open tubular column, again a decrease in lag time and steady state thermal offset

was noted, attributed to the increased heat transfer across the liquid layer. The same conclusions can be made for other LC solvents such as acetonitrile and methanol compared to water (used in the present study).

The air gap between the inner surface of the aluminium heating sleeve and the outer surface of the capillary was found to be the rate determining step of the heat transfer, as the thickness of the air layer largely affects the thermal lag time and the steady state thermal offset value. When filling the air gap with thermal paste, an enhancement of the heat transfer was noted, leading to a reduction of the steady state thermal offset value of 1 K.

The band broadening caused by the radial temperature gradients inside the liquid layer was calculated from the temperature profiles derived with the infinitely long cylinder model (analytical model) applied to the liquid zone only. It was found that for a given temperature ramp, the expected contribution to band broadening is negligible for capillaries with a sufficiently small inner diameter, but increases steeply at a given critical diameter. This 'critical' diameter depends on the applied temperature ramp, but also on the mobile phase solvent and the retention enthalpy of the molecules. For a temperature ramp of 1 K/s, 2.1 mm narrow-bore columns can still be used (solvents water, acetonitrile and methanol), but for a temperature ramp of 10 K/s, the column inner diameter should not exceed 900–1000 μm (acetonitrile and methanol) or 1100–1200 μm (water) in order to avoid excessive band broadening (calculated values for a packed bed and a retention enthalpy of −15 kJ/mol). For more temperature sensitive molecules such as macromolecules, the contribution to band broadening will even be larger and capillaries with smaller inner diameters should be used.

Symbol list

A_{ax}	axial surface of numerical simulation cell [m^2]
A_{rad}	radial surface of numerical simulation cell [m^2]
C_p	heat capacity [J/kg K]
$C_{p,v}$	thermal mass [J/m^3 K]
d_p	particle diameter [m]
D	radial dispersion coefficient
D_{rad}	radial diffusion coefficient [m^2/s]
F	flow rate [μl/min]
H_{extra}	contribution to the plate height [m]
H_{min}	plate height at the optimal velocity [m]
ΔH_R	retention enthalpy [J/mol]
i.d.	inner diameter [m]
J_n	nth order Bessel function
o.d.	outer diameter [m]
r	radius [m]
r_{id}	inner radius of capillary [m]
r_{od}	outer radius of capillary [m]
R	radius of total setup [m]
R_g	universal gas constant
t	time [s]
t_{delay}	delay time [s]
t_{lag}	lag time [s]
T	temperature [K]
T_0	initial temperature [K]
$T_{axis,liq}$	temperature of the liquid at the middle of the capillary [K]
$T_{wall,liq}$	temperature of the liquid at the inner surface of the capillary [K]
$T_{liq,ave}$	average temperature of liquid [K]
T_{sleeve}	temperature of heating sleeve [K]
ΔT_{ss}	steady state temperature offset [K]
$\Delta T_{max,liq}$	maximal temperature gradient in liquid [K]
u	mobile phase velocity [m/s]
u_{0m}	mean velocity of unretained species [m/s]
$u_{0,wall}$	velocity of unretained species near column wall [m/s]
u_{Rm}	mean velocity of retained species [m/s]
u_{Rw}	velocity of retained species near column wall [m/s]
V_{cell}	volume of numerical simulation cell [m^3]

Greek symbols

α	thermal diffusivity [m^2/s]
β	temperature ramp [K/s]
ε	porosity
η	viscosity [Pa s]
κ	geometrical Aris constant
λ	thermal conductivity [W/m K]
ρ	density [kg/m^3]

Subscripts

TP	thermal paste layer
air	air layer
OT	open-tubular column
PB	packed bed column

Acknowledgements

M.V. gratefully acknowledges a research grant from the Research Foundation–Flanders (FWO Vlaanderen). Agilent Technologies (Hans-Georg Weissgerber, Tom Vandegoor, Gerard Rozing, Monika Dittmann and Helmut Schulenberg-Schell) is kindly thanked for experimental support and stimulating discussions on this project.

References

[1] M. Gilar, U.D. Neue, J. Chromatogr. A 1169 (2007) 139.
[2] D. Cabooter, J. Billen, H. Terryn, F. Lynen, P. Sandra, G. Desmet, J. Chromatogr. A 1204 (2008) 1.
[3] J.E. MacNair, K.D. Patel, J.W. Jorgenson, Anal. Chem. 71 (1999) 700.
[4] K.J. Fountain, U.D. Neue, E.S. Grumbach, D.M. Diehl, J. Chromatogr. A 1216 (2009) 5979.
[5] F.D. Antia, C. Horvath, J. Chromatogr. 435 (1988) 1.
[6] D. Guillarme, S. Heinisch, J.L. Rocca, J. Chromatogr. A 1052 (2004) 39.
[7] S. Heinisch, G. Desmet, D. Clicq, J.L. Rocca, J. Chromatogr. A 1023 (2008) 124.
[8] S. Heinisch, J.L. Rocca, J. Chromatogr. A 1216 (2009) 642.
[9] G. Vanhoenacker, P. Sandra, Anal. Bioanal. Chem. 390 (2008) 245.
[10] G. Vanhoenacker, P. Sandra, J. Sep. Sci. 29 (2006) 1822.
[11] H. Poppe, J.C. Kraak, J. Chromatogr. 282 (1983) 399.
[12] T. Welsch, M. Schmid, J. Kutter, A. Kálmán, J Chromatogr. A 728 (1996) 299.
[13] R.G. Wolcott, J.W. Dolan, L.R. Snyder, S.R. Bakalyar, J. Chromatogr. A 869 (2000) 211.
[14] G. Desmet, J. Chromatogr. A 1116 (2006) 89.
[15] F. Gritti, G. Guiochon, J. Chromatogr. A 1138 (2007) 141.
[16] D. Cabooter, F. Lestremau, A. de Villiers, K. Broeckhoven, F. Lynen, P. Sandra, G. Desmet, J. Chromatogr. A 1216 (2009) 3895.
[17] M.M. Fallas, M.R. Hadley, D.V. McCalley, J. Chromatogr. A 1216 (2009) 3961.
[18] L.R. Snyder, J. Chromatogr. 13 (1964) 415.
[19] C.F. Poole, S.K. Poole, Chromatography Today, Elsevier, Amsterdam, 1991.
[20] M.H. Chen, C. Horvath, J. Chromatogr. A 788 (1997) 51.
[21] T. Greibrokk, T. Andersen, J. Sep. Sci. 24 (2001) 899.
[22] T. Teutenberg, Anal. Chim. Acta 643 (2009) 1.
[23] B. Gu, H. Cortes, J. Luong, M. Pursch, P. Eckerle, R. Mustacich, Anal. Chem. 81 (2009) 1488.
[24] S. Giegold, T. Teutenberg, J. Tuerk, T. Kiffmeyer, B. Wenclawiak, J. Sep. Sci. 31 (2008) 3497.
[25] F. Houdiere, P.W.J. Fowler, N.M. Djordjevic, Anal. Chem. 69 (1997) 2589.
[26] A. Pappa-Louisi, P. Nikitas, C. Zisi, K. Papachristos, J. Sep. Sci. 31 (2008) 2953.
[27] P. Nikitas, A. Pappa-Louisi, K. Papachristos, C. Zisi, Anal. Chem. 80 (2008) 5508.
[28] A. Pappa-Louisi, P. Nikitas, K. Papachristos, C. Zisi, Anal. Chem. 81 (2009) 1217.
[29] E. Landberg, A. Lundblad, P. Pahlsson, J. Chromatogr. A 814 (1998) 97.
[30] S.M.C. Buckenmaier, D.V. McCalley, M.R. Euerby, J. Chromatogr. A 1060 (2004) 117.
[31] Y.Q. Xiang, B.W. Yan, B.F. Yue, C.V. McNeff, J. Chromatogr. A 983 (2003) 83.
[32] K. van Lenning, J.L. Garrido, J. Aristegui, M. Zapata, Chromatographia 41 (1995) 539.
[33] W.S. Hancock, R.C. Chloupek, J.J. Kirkland, L.R. Snyder, J. Chromatogr. A 686 (1994) 31.
[34] W.H. Braunlin, I. Giri, L. Beadling, K.J. Breslauer, Biopolymers 74 (2004) 221.
[35] The Selerity Technologies website, http://www.selerity.com.
[36] The Scientific Instruments Manufacturer website, http://www.sim-gmbh.de.

[37] J. Bullock, J. Chromatogr. A 694 (1995) 415.
[38] T. Teutenberg, H.-J. Goetze, J. Tuerk, J. Ploeger, T.K. Kiffmeyer, K.G. Schmidt, W.Gr. Kohorst, T. Rohe, H.-D. Jansen, H. Weber, J. Chromatrogr. A 1114 (2006) 89.
[39] T.S. Kephart, P.K. Dasgupta, Anal. Chim. Acta 414 (2000) 71.
[40] T. Andersen, P. Molander, R. Trones, D.R. Hegna, T. Greibrokk, J. Chromatogr. A 918 (2001) 221.
[41] R. Mustacich, J. Richards, J. Everson, U.S. Patent 6.530.260 (2003).
[42] R. Mustacich, J. Everson, U.S. Patent 6.682.699 (2004).
[43] H.S. Carslaw, J.C. Jaeger, Conduction of Heat in Solids, 2nd ed., Clarendon Press, Oxford, 1986.
[44] M. Abramowitz, I. Stegun, Handbook of Mathematical Functions with Formulas, Graphs and Mathematical Tables, 9th printing, Dover, New York, 1972.
[45] H. Gerber, Math. Comput. 18 (1964) 319.
[46] J.H. Knox, I. Grant, Chromatographia 24 (1987) 135.
[47] H. Poppe, J.C. Kraak, J.F.K. Huber, J.H.M. van den Berg, Chromatographia 14 (1981) 515.
[48] H. Vogel, Physik Z 22 (1921) 645.
[49] G.S. Fulcher, J. Am. Ceram. Soc. 8 (1925) 339.
[50] G. Tammann, W. Hesse, Z. Anorg, Allg. Chem. 156 (1926) 245.
[51] Y.S. Touloukian, S.C. Saxena, P. Hestermaus, Thermophysical Properties of Matter—TPRC Data Series. II. Viscosity, Purdue Research Foundation, 1975.
[52] J. Billen, K. Broeckhoven, A. Liekens, K. Choikhet, G. Rozing, G. Desmet, J. Chromatogr. A 1210 (2008) 30.
[53] R.B. Bird, W.E. Stewart, E.N. Lightfoot, Transport Phenomena, Wiley, New York, 1960.
[54] R. Aris, Proc. R. Soc. A 235 (1956) 67.
[55] Thermal grease datasheet, found at http://www2.produktinfo.conrad.com/datenblaetter/175000-199999/189070-da-01-en-WL_DISP_KP92_WAERMELEITP_3_ML.pdf.
[56] H. Kadokura, H. Yokokawa, Y. Takahashi, Netsusokutei 4 (1977) 52.
[57] J.D. Thompson, J.S. Brown, P.W. Carr, Anal. Chem. 73 (2001) 3340.
[58] J. Billen, G. Desmet, J. Chromatogr. A 1168 (2007) 73.
[59] Y.P. Zarichnyak, V.V. Novikov, Inzh. -Fizi. Zh. 34 (1978) 648.
[60] F. Gritti, G. Guiochon, Anal. Chem. 80 (2008) 5009.
[61] J.H. Knox, G.R. Laird, P.A. Raven, J. Chromatogr. 122 (1976) 129.
[62] U. Tallarek, K. Albert, E. Bayer, G. Guiochon, AIChE J. 41 (1996) 3041.
[63] P. Molander, R. Olsen, E. Lundanes, T. Greibrokk, Analyst 128 (2003) 1341.
[64] P. Szabelski, A. Cavazzini, K. Kaczmarski, X. Liu, J. Van Horn, G. Guiochon, J. Chromatogr. A 950 (2002) 41.
[65] CRC Handbook of Chemistry and Physics, 87th ed., CRC Press, 2006.